

## Force Field of Monoethanolamine

José Alejandro,<sup>\*,†,‡</sup> José Luis Rivera,<sup>†</sup> Marco Antonio Mora,<sup>†</sup> and Virgínia de la Garza<sup>†</sup>

*Departamento de Química, Universidad Autónoma Metropolitana-Iztapalapa, Apdo. Postal 55-534, 09340 México D.F., México, and Simulación Molecular, Instituto Mexicano del Petróleo, Eje Central Lázaro Cárdenas 152, Apdo. Postal 14-805, 07730 México D.F., México*

*Received: September 1, 1999; In Final Form: November 17, 1999*

We have performed ab initio calculations and canonical molecular dynamics simulations to obtain a force field of monoethanolamine (MEA). The molecule is modeled by seven charged sites, and the force field includes intramolecular degrees of freedom and intermolecular interactions. The charges obtained in the energy minimization procedure reproduce the experimental geometry, dipole moment, and the most stable conformation. Molecular dynamics simulations were carried out in the liquid phase and in the liquid–vapor equilibrium state. Simulations in the liquid region give us information about hydrogen bond formation, while simulations in the two-phase region allow us to obtain the coexisting densities and surface tension as functions of temperature. The hydrogen bond is favored when the hydrogen of the hydroxyl group is close to a nitrogen or to an oxygen of another molecule, and the strength in both cases is the same. Radial distribution functions involving hydrogens and oxygen in the hydroxyl group of MEA are compared with those of water at 298 K, and a similar structure is found for the first neighbor of atoms. The proposed force field gives a good description of the liquid–vapor coexistence of MEA. The liquid density obtained in our simulations of the liquid–vapor equilibrium at 298 K is 1.003 g/cm<sup>3</sup> versus the experimental value of 1.012 g/cm<sup>3</sup>. Our estimated critical point is located at 583.9 K and 0.32 g/cm<sup>3</sup> in comparison with the experimental result of 614 K and 0.3116 g/cm<sup>3</sup>, respectively. At 323 K the calculated surface tension is 43.2 ± 2.5 mN/m while the experimental value is 44.81 mN/m.

### I. Introduction

Aqueous solutions of alkanolamines are used in the petroleum industry to remove acid gases from natural gas in refining and purification processes. They are attractive owing to their low cost and their ability to absorb acid gases. They are also used in the detergent and textile industries.<sup>1</sup> Alkanolamines are organic polar molecules that contain an alcohol and an amine group; their generalized formula is NH<sub>3-*n*</sub>(C<sub>2</sub>H<sub>4</sub>OH)<sub>*n*</sub>. When *n* is unity, the chemical is called monoethanolamine, MEA, or 2-aminoethanol. Alkanolamines are mainly used in aqueous solutions to eliminate H<sub>2</sub>S and CO<sub>2</sub> from natural gas streams. Their concentration in solution varies from 10 to 30% in mass.<sup>1</sup> Precise knowledge of the thermophysical properties of alkanolamine solutions is important for designing and operation of refining and purification processes.

Some experimental data are available for MEA and diethanolamine (DEA), both pure and in aqueous solutions. Normal densities, viscosities, surface tensions, and other thermophysical properties<sup>2–6</sup> have been reported for liquid conditions. The geometry and dipole moment of MEA have been determined by spectroscopic methods.<sup>7</sup>

Unfortunately, experimental data are scarce for higher alkanolamines. Furthermore, they are generally used in multicomponent mixtures. Such mixtures are highly nonideal; it is difficult to predict their thermodynamic and transport properties using conventional engineering methods. Quantitative methods for prediction of such properties would be of considerable use to the petroleum industry. It is our interest to conduct a systematic investigation of thermodynamic and transport properties of aqueous solutions of alkanolamines in one and two phases.

This is an area where quantum mechanical and computer simulation methods can help one to understand the effect that molecular interactions have on such properties.

Actually, there are fairly good potentials to simulate water in one and two phases.<sup>8,9</sup> To be able to simulate aqueous solutions of alkanolamines, we have to develop the corresponding force field for pure alkanolamines. We have chosen MEA to start our investigation.

Recently, Button et al.<sup>10</sup> used molecular dynamics simulations to study hydrogen bonding in liquid MEA. Those authors employed a force field that is a combination of those reported for alcohols and amines. Unfortunately, they did not compare their results with experimental data. The electrostatic interactions were shifted to zero with a smooth function; it is therefore not possible to draw any conclusions regarding the accuracy of their model.

In this work we develop a force field for MEA combining ab initio calculations and molecular dynamics simulations. The potential includes intramolecular and intermolecular interactions. Using ab initio calculations, we obtained the geometry of MEA, the bending and torsional energy, and the charges. The calculated charges reproduce the experimental dipole moment. The potential was validated by doing molecular dynamics simulations in the liquid–vapor interface in order to obtain coexisting densities and surface tension as functions of temperature.

There are different methods to directly study fluid-phase equilibria with a small number of simulations. Representative methods are the Gibbs ensemble<sup>11</sup> and its extensions,<sup>12</sup> the Gibbs–Duhem,<sup>13</sup> the canonical Monte Carlo (CMC),<sup>14</sup> and molecular dynamics (CMD).<sup>15,16</sup> We have recently shown<sup>17</sup> for Lennard-Jones fluids that when the same potential model is used, CMC and CMD simulations of interfaces produce the same results for coexisting densities and vapor pressures as other

<sup>†</sup> Universidad Autónoma Metropolitana-Iztapalapa.

<sup>‡</sup> Instituto Mexicano del Petróleo.

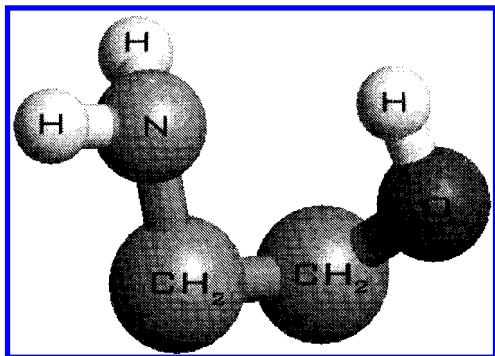


Figure 1. Molecular geometry of MEA.

methods used to simulate phase equilibria, but where the interface is not present. In this work we have used direct canonical molecular dynamics simulations of interfaces to calculate the coexisting densities and surface tension of MEA in the liquid–vapor equilibrium. This method has been successfully applied to study phase equilibria of molecular systems such as water,<sup>15</sup> small hydrocarbons,<sup>18</sup> oligomers,<sup>16</sup> water–methanol mixtures,<sup>19,20</sup> and perfluoroalkanes.<sup>21</sup>

The article is organized as follows: Ab initio calculations and the potential model are described in section 2. In section 3 we give the simulation details. Results of liquid-phase simulations are in section 4, while in section 5 liquid–vapor simulations results are shown. Finally, conclusions and references are given.

## II. Potential Model

Monoethanolamine molecules are modeled using a united atom model for the CH<sub>2</sub> groups. The molecule contains, as shown in Figure 1, seven charged sites: three hydrogens, one nitrogen, one oxygen, and two CH<sub>2</sub> pseudoatoms.

The geometry of MEA was obtained by means of the SPARTAN package<sup>22</sup> using the AM1 method as a starting point. The geometry was reoptimized using the Gaussian94 package<sup>23,24</sup> with a chemistry model HF/STO-3G, and the charges were calculated using the electrostatic potential criteria and produced a dipole moment of 3.259 D, which compares favorably with the experimental value of 3.05 D.<sup>7</sup> The final geometry was reoptimized using Gaussian94 with a more accurate optimization HF/6-311+G(2d,p). The new charges gave a dipole moment of 3.044 D and reproduced the experimental geometry and the most stable conformation.<sup>7</sup> The calculated nitrogen–oxygen distance within a molecule is 2.86 Å, in good agreement with the experimental value of 2.81 Å.<sup>25</sup>

During the simulations the bond distances were kept constant at their equilibrium value by using a SHAKE procedure.<sup>26</sup> This allowed us to eliminate short-time vibrations and to increase the time step necessary to integrate the classical equations of motion.

The intramolecular interactions are given by harmonic type potentials for bond angles

$$U(\theta) = \frac{k_\theta}{2} (\theta - \theta_0)^2 \quad (1)$$

where  $\theta$  is the bond angle, the subscript 0 denotes its equilibrium value, and  $k_\theta$  is the spring constant, obtained using Gaussian94. The method HF/6-31G\* was used to obtain the energy as a function of the bond angle. The energy was calculated in a range of  $\pm 10^\circ$  around  $\theta_0$  in increments of  $1^\circ$ . The spring constant was obtained by fitting a quadratic function to the results of energy calculations.

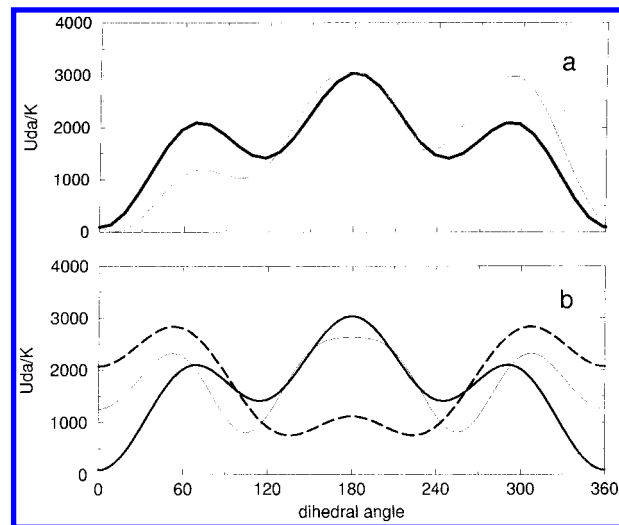


Figure 2. Torsional angle potentials of MEA. (a) Comparison between ab initio (thin line) and eq 2 (solid line) results for  $\phi_1$ . (b) Fitted results: solid line for  $\phi_1$ , thin line for  $\phi_2$ , and dashed line for  $\phi_3$ .

The torsional angle energies around the bonds N–C, C–C, and C–O are given by

$$U(\phi) = \sum_{i=0}^5 C_i \cos(\phi)^i \quad (2)$$

where  $\phi$  is the torsional angle between four atoms and  $C_i$  are constants. To obtain the  $C_i$  values we performed ab initio calculations for every torsional angle using Gaussian94 with a basis set 6-31G\*. The energy was obtained in the whole range of torsions, from 0 to  $360^\circ$ , in increments of  $10^\circ$ . A periodic function given by eq 2 was fitted to the energy, and the constants were thus obtained. In eq 2 we used the convention that trans and cis conformations occur when  $\phi$  is equal to 0 and  $180^\circ$ , respectively.

Figure 2a shows the potential energy as a function of  $\phi$  for the HN–CC torsion obtained from ab initio calculations and using eq 2. The maxima and minima lie near the same angle, and the fitted results are symmetric around  $180^\circ$ . Figure 2b shows adjusted results for the three torsional angles in the molecule ( $\phi_1$ , HN–CC;  $\phi_2$ , NC–CO;  $\phi_3$ , CC–OH). We can see that the more stable conformation occurs for  $\phi_1 = 0^\circ$ ,  $\phi_2 = 100^\circ$ , and  $\phi_3 = 130^\circ$  in fairly good agreement with experimental results<sup>7</sup> where the most stable conformation is  $\phi_1 = 20.5^\circ$ ,  $\phi_2 = 124.6^\circ$ , and  $\phi_3 = 151.7^\circ$ .

The intermolecular interactions are given by the truncated and shifted Lennard-Jones and by the Coulomb potentials for the short- and long-range interactions, respectively. The interaction between atom  $a$  in molecule  $i$  and atom  $b$  in molecule  $j$  is given by

$$U(r_{iajb}) = 4\epsilon \left[ \left( \frac{\sigma}{r_{iajb}} \right)^{12} - \left( \frac{\sigma}{r_{iajb}} \right)^6 \right] + \frac{q_{ia}q_{jb}}{r_{iajb}} \quad (3)$$

where  $\sigma$  is the diameter of a site,  $\epsilon$  is the well depth,  $q_{ia}$  is the charge of atom  $a$  in molecule  $i$ , and  $r_{iajb}$  is the distance between site  $a$  in molecule  $i$  and site  $b$  in molecule  $j$ .

The  $\sigma$  and  $\epsilon$  parameters for the non-hydrogen sites were taken from ref 10. The charges for each site were obtained from ab initio calculations as explained above. The parameters used in eqs 1–3 are given in Table 1.

The Lorentz–Berthelot mixing rule was used for atoms of different types.

**TABLE 1: Potential Parameters of MEA**

Bond Distances									
site		site	$r_0$ (Å)						
H		N	1.00						
N		C	1.44						
C		C	1.54						
C		O	1.42						
O		H	0.96						
Bond Angles									
site		site	site	$k_\theta$ (K rad <sup>-2</sup> )	$\theta_0$				
H		N	H	64 796.57	108.48				
H		N	C	76 164.39	110.35				
N		C	C	121 761.97	116.68				
C		C	O	131 550.93	107.30				
C		O	H	71 869.88	106.80				
Torsional Angles ( $C_i$ are given in K)									
$i$	$j$	$k$	$l$	$C_0$	$C_1$	$C_2$	$C_3$	$C_4$	$C_5$
H	N	C	C	1795.46	1329.17	-285.31	-3042.66	51.83	242.38
N	C	C	O	1106.49	2138.57	2838.57	-4426.86	-2000.71	1602.44
C	C	O	H	1943.73	2302.59	-335.30	-1636.87	-14.44	-186.10
Lennard-Jones Parameters and Charges <sup>a</sup>									
site		site	$\sigma$		$\epsilon/\kappa$		$q$		
HN		HN	0		0		0.347		
N		N	3.250		85.51		-0.938		
C		C	3.905		59.42		0.257		
O		O	3.070		85.51		-0.644		
HO		HO	0		0		0.374		

<sup>a</sup> The units of  $\sigma$  are angstroms,  $\epsilon/k$  are kelvins, and charges are in electrons. HN means hydrogen bonded to nitrogen.

### III. Simulation Details

In this work we have carried out canonical molecular dynamics simulations in the liquid phase and in the liquid–vapor equilibrium to obtain structural and thermodynamic properties of MEA. All simulations were performed using the Verlet algorithm at constant temperature. The electrostatic interactions were handled by an Ewald summation technique. The use of a neighbor list allows us to reduce the computing time, mainly in the two-phase simulations where large systems are needed. In the liquid simulations the number of molecules is 250 and 500 in the two-phase systems. In both cases the temperature covers the range between 298 and 530 K, which is between the triple and the critical points of MEA.

The truncation of the short-range interaction is performed at 11.0 Å and at 14.5 Å in the liquid and the two-phase simulations, respectively. To simulate the liquid–vapor phase equilibrium of MEA, we allocated in the Z-direction 500 molecules in the center of a parallel piped cell surrounded by vacuum and then the system was equilibrated. This is a common way of setting up the initial configuration when interfaces are being simulated.<sup>15</sup> The dimensions of the simulation cell are  $L_x = L_y = 37.8348$  Å and  $L_z = 113.5$  Å. In all simulations the time step was 1.0 fs. The  $\kappa$  parameter in the Ewald sum was  $5.6/L_x$ , and  $h_{\max}$  was given a maximum value of 8. After an equilibration period of 20 000 steps for liquid simulations and 50 000 for the two-phase systems, the average properties were obtained for further 50 000 steps and 350 000 steps for the one- and the two-phase simulations, respectively. The temperature was kept constant by rescaling velocities every configuration.

The molecular density profile was obtained by

$$\langle \rho(z) \rangle = \frac{\langle N(z) \rangle}{A \Delta z} \quad (4)$$

where  $N(z)$  is the number of molecules in a slab located between

$z$  and  $z + \Delta z$ ,  $A$  is the surface area,  $A = L_x L_y$ , and  $\Delta z$  is the width of the slab. In this work,  $\Delta z$  is 0.2 Å. The brackets denote time averaging.

The liquid and vapor densities were obtained by fitting a hyperbolic tangent function to the density profile

$$\rho(z) = \frac{1}{2}(\rho_L + \rho_V) - \frac{1}{2}(\rho_L - \rho_V) \tanh \left[ \frac{z - z_0}{d} \right] \quad (5)$$

where  $\rho_L$  and  $\rho_V$  are the liquid and vapor densities, respectively,  $z_0$  is the Gibbs' dividing surface, and  $d$  is a measure of the width of the interface.

By changing the temperature, we were able to build up the whole envelope of the coexisting phases.

The calculated coexisting densities were used to estimate the critical parameters of MEA. We used the scaling law of densities and rectilinear diameter law with the first three terms of a Wegner expansion<sup>27</sup> of the form

$$\rho_{\pm} = \rho_C + C_2 |t| \pm (B_0 |t|^\beta + B_1 |t|^{\beta+(1/2)}) \quad (6)$$

where  $\rho_-$  and  $\rho_+$  represent the vapor- and liquid-phase densities,  $\beta = 0.325$  is a universal critical exponent determined from the renormalization group theory, and  $t = 1 - T/T_C$  where  $T$  is the absolute temperature. The critical density and temperature are  $\rho_C$  and  $T_C$ , respectively.

The surface tension can be calculated using the mechanical definition of the molecular pressure tensor. The intramolecular interactions, in this case, do not contribute to the surface tension. The procedure used in this work is the same as that used to simulate the liquid–vapor interface of water<sup>15</sup> and *n*-hexane.<sup>18</sup> The molecular surface tension is defined in terms of pressure tensor components as

$$\gamma = \frac{L_z}{2} \left[ \langle P_{zz} \rangle - \frac{1}{2} (\langle P_{xx} \rangle + \langle P_{yy} \rangle) \right] \quad (7)$$

where  $P_{\alpha\alpha}$  is the  $\alpha\alpha$  element of the pressure tensor and  $L_z$  is the magnitude of the cell length in the Z-direction. The factor (1/2) outside the bracket takes into account the fact that we have two interfaces. The element  $P_{\alpha\beta}$  of the molecular pressure tensor for additive pair potentials, as is the case of the Lennard-Jones, is

$$VP_{\alpha\beta} = \sum_i M_i (\mathbf{V}_i)_\alpha (\mathbf{V}_i)_\beta + \sum_i \sum_{j>i} \sum_a \sum_b (\mathbf{R}_{ij})_\alpha (\mathbf{F}_{iajb})_\beta \quad (8)$$

where  $N$  is the number of molecules,  $V$  is the volume of the system,  $M_i$  is the molecular mass,  $(\mathbf{V}_i)_\alpha$  is the velocity of the center of mass in the  $\alpha$  direction,  $(\mathbf{R}_{ij})_\alpha$  is the distance between the centers of mass of molecules  $i$  and  $j$  in the  $\alpha$  direction, and the force between atom  $a$  in molecule  $i$  and atom  $b$  in molecule  $j$  is

$$\mathbf{F}_{iajb} = -\frac{\mathbf{r}_{iajb}}{r_{iajb}} \left[ \frac{dU(r_{iajb})}{dr_{iajb}} \right] \quad (9)$$

For the Coulomb interactions treated with the Ewald sum, the reciprocal space contribution is not pairwise additive; thus, eq 9 cannot be applied. The components of the pressure tensor of electrostatic interactions have been already obtained,<sup>15,18</sup> and for completeness we give the basic equations

$$VP_{\alpha\beta} = \sum_i \sum_a q_{ia} \sum_{j>i} \sum_b q_{ib} \left[ \frac{2}{\sqrt{\pi}} \kappa r_{iajb} \exp(-\kappa^2 r_{iajb}^2) + \operatorname{erfc}(\kappa r_{iajb}) \right] \frac{(\mathbf{R}_{ij})_\alpha (\mathbf{r}_{iajb})_\beta}{r_{iajb}^3} + \frac{2\pi}{V} \sum_{\mathbf{h} \neq 0} Q(h) S(\mathbf{h}) S(-\mathbf{h}) \left( \delta_{\alpha\beta} - \frac{2\mathbf{h}_\alpha \mathbf{h}_\beta}{h^2} - \frac{2\mathbf{h}_\alpha \mathbf{h}_\beta}{h^2} - \frac{\mathbf{h}_\alpha \mathbf{h}_\beta}{2\kappa^2} \right) - \sum_i \sum_a (\mathbf{r}_{ia} - \mathbf{r}_i)_\beta (\mathbf{F}_{ia}^K)_\alpha \quad (10)$$

where  $S(\mathbf{h})$  and  $Q(h)$  are

$$S(\mathbf{h}) = \sum_i \sum_a q_{ia} \exp(i\mathbf{h} \cdot \mathbf{r}_{ia}) \quad (11)$$

$$Q(h) = \exp(-h^2/4\kappa^2)/h^2 \quad (12)$$

with  $\mathbf{h}$  being the reciprocal lattice vector. The force of the reciprocal space part is given by

$$\mathbf{F}_{ia}^K = \frac{4\pi q_{ia}}{V} \sum_{\mathbf{h} \neq 0} Q(h) \mathbf{h} \operatorname{Imag}[\exp(-i\mathbf{h} \cdot \mathbf{r}_{ia}) S(\mathbf{h})] \quad (13)$$

where  $\operatorname{Imag}$  denotes the imaginary part of the complex variable.

The long-range corrections to the surface tension for intermolecular dispersion interactions were obtained according to the description given in ref 18. The assumption was made that the density profile of every atom in MEA was the same as that of the molecular center of mass and that  $\rho(z)$  can be fitted to a hyperbolic tangent function. The correction is

$$\gamma_{\text{LRC}} = 12\pi(\rho_L - \rho_V)^2 \sum_{a=1}^n \sum_{b=1}^n \epsilon_{ab} \sigma_{ab}^6 \int_0^1 ds \int_{R_c}^\infty dr \coth \left( \frac{rs}{d} \right) \frac{(3s^3 - s)}{r^3} \quad (14)$$

where  $\rho_L$  and  $\rho_V$  are the molecular liquid and vapor densities, respectively,  $d$  is a measure of the width of the interface, and  $R_c$  is the cutoff distance. For MEA,  $n$  takes a value of 5 in eq 14 because only five sites have Lennard-Jones interactions.

#### IV. Liquid-Phase Results

This section contains results for pure MEA in the liquid phase. Simulations were carried out along the simulated coexistence curve. The intramolecular and intermolecular contributions to the potential are given in Table 2. As expected, the intramolecular contribution increases with temperature while the intermolecular potential becomes less negative. Figure 3 shows the calculated torsional angle distribution at 350 K. It can be seen that molecules are, on the average, in the most stable conformation.

Monoethanolamine has seven charged sites and, in the liquid phase, associates to form hydrogen bonds. MEA has a density of 1.018 g/cm<sup>3</sup> at room temperature, and its boiling temperature is 445 K at normal pressure. To analyze the formation of hydrogen bonds, we performed simulations in the liquid phase at different temperatures along the orthobaric curve. We calculated the intermolecular radial distribution functions that involve sites H, O and N. The results of  $g_{\text{O-HO}}(r)$ ,  $g_{\text{N-HO}}(r)$ ,  $g_{\text{O-HN}}(r)$ , and  $g_{\text{N-HN}}(r)$  at 298 and 400 K are shown in Figure 4. The  $g_{\text{X-HY}}(r)$  is the probability of atom X in one molecule associating with a hydrogen bonded to an atom Y of another molecule. In our case, X and Y can be oxygen or nitrogen. The first maximum in Figure 4a,b gives the probability of finding a

TABLE 2: Thermodynamic Properties of MEA<sup>a</sup>

T	$\rho$	$U(\text{intra})$	$U(\text{inter})$
298	1.003	26.985	-55.378
350	0.939	29.427	-49.300
400	0.870	31.386	-43.065
450	0.795	33.706	-37.547
500	0.700	36.092	-31.327
550	0.483	38.154	-22.840

<sup>a</sup> Given are the temperature, the liquid density, and the intramolecular and intermolecular contributions to the potential. The units of temperature are kelvin, the density is given in g/cm<sup>3</sup>, and energy is in kJ/mol.

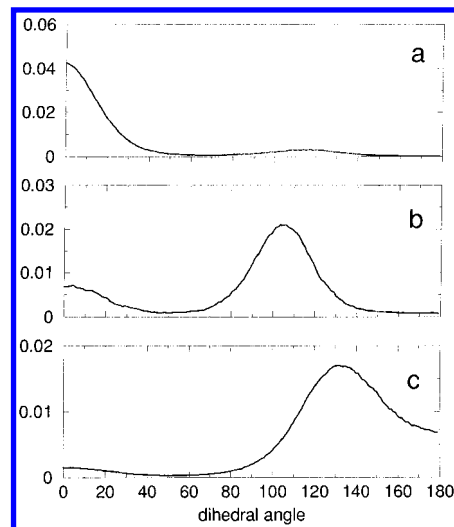


Figure 3. Rotational angle distributions of liquid MEA obtained using CMD at 350 K and 0.939 g/cm<sup>3</sup>: (a) HNNC, (b) NCCO and (c) CCOH.

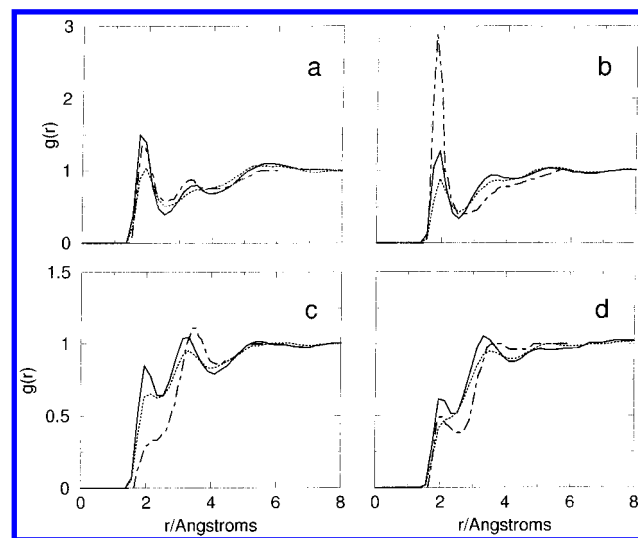
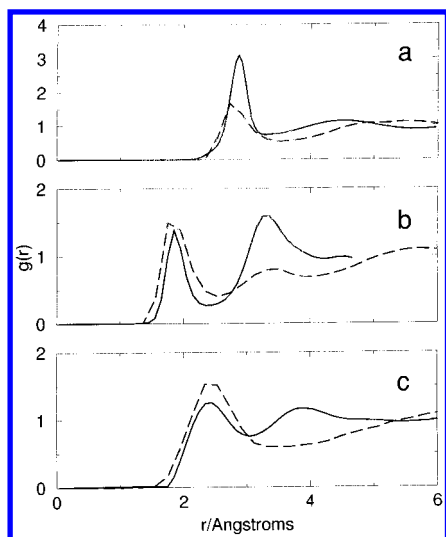


Figure 4. Intermolecular radial distribution functions at 298 K (solid line) and 400 K (dashed line) of this work. Results with dot-dashed line are from ref 10 at 390 K: (a) O-HO, (b) N-HO, (c) N-HN, and (d) O-HN.

hydrogen of the hydroxyl group around 1.8 Å from a nitrogen or oxygen of another molecule. The hydrogen of the hydroxyl group associates electrostatically with a nitrogen of the amino group and with the oxygen of the hydroxyl group. Clearly the hydrogen bond between oxygen and nitrogen is favored when they are close to a hydrogen of the hydroxyl group (see Figure 4a,b). The hydrogen in the amino group does not favor the hydrogen bonding with an oxygen or nitrogen from another molecule, as shown in Figure 4c,d. As expected, the hydrogen bond is weaker at 400 K. The same behavior has been observed





**Figure 5.** Radial distribution functions of MEA (dashed line) and water from ref 29 (solid line): (a) O–O, (b) O–H, and (c) H–H.

in water.<sup>28</sup> In this work the radial distribution functions have the same trend as found in ref 10, as shown in Figure 4 by a dot–dashed line, but in our case the first maximum in  $g_{N-HO}(r)$  and  $g_{O-HO}(r)$  has almost the same value, while in ref 10 the first maximum of  $g_{N-HO}(r)$  is twice that of  $g_{O-HO}(r)$ . Although our results cannot be compared at the same conditions, in that article  $g_{N-HO}(r)$  at 390 K has a first maximum almost twice that of the results of this work at 298 K. Because in their calculation was used a higher temperature, this peak should be lower.

Water and MEA have different numbers of atoms and therefore different geometry; however, some properties are similar. At 298 K, water has a density of 0.998 g/cm<sup>3</sup> and MEA 1.012 g/cm<sup>3</sup>, the critical point of water is  $\rho_c = 0.3155$  g/cm<sup>3</sup> and  $T_c = 647.3$  K; for MEA the critical point is  $\rho_c = 0.3116$  g/cm<sup>3</sup> and  $T_c = 614$  K.<sup>2</sup> Differences are found in the viscosity, (0.9 cP for water and 19 cP for MEA) and the boiling point (373 K for water and 443.5 K for MEA). In the absence of experimental results for the radial distribution functions of MEA, and because of its similar properties to water, we compare at 298 K the experimental  $g_{O-O}(r)$ ,  $g_{O-H}(r)$ , and  $g_{H-H}(r)$  of water with the calculated values of the hydroxyl group in MEA; the results are shown in Figure 5. We can see that the first peak in the three radial distribution functions of MEA lies around the same position as those of water. Because of the length of MEA and because oxygen has one hydrogen bonded, the first maximum in  $g_{O-O}(r)$  is lower than that in water. Figure 5b shows a comparison between  $g_{O-H}(r)$  of MEA and water. The first maximum gives the hydrogen bond formation. It is slightly higher in MEA than in water. The hydrogen bond in MEA has the N–HO and the O–HO contributions at 298 K; they are about the same (see Figure 4a,b), thus the hydrogen bond interaction in MEA is almost twice that in water. These results might be used to explain why MEA has a higher boiling temperature than water.

## V. Liquid–Vapor Equilibrium Results

To test the force field of MEA, we carried out CMD simulations in the liquid–vapor equilibrium. In CMD calculations of interfaces it is not clear how to properly include long-range corrections to the forces. The simulation is thus performed with a truncated and shifted potential using a large cutoff distance. There is not a direct way of extrapolating the densities

**TABLE 3: Liquid and Vapor Coexisting Densities of MEA<sup>a</sup>**

$T$	$\rho_v$	$\rho_L$	$\gamma(\text{MD})$	$\gamma(\text{tail})$	$\gamma$
298	0.0001	1.003	41.5	6.9	48.4
323	0.0002	0.973	36.8	6.4	43.2
350	0.0005	0.939	31.0	6.0	37.0
400	0.0023	0.870	24.5	4.9	29.4
450	0.0152	0.795	16.0	3.8	19.8
500	0.0520	0.700	6.5	2.0	8.5
530	0.0710	0.637			

<sup>a</sup> The calculated surface tension is  $\gamma(\text{MD})$ ;  $\gamma(\text{tail})$  is the long range correction to the surface tension obtained with eq 14 and  $\gamma = \gamma(\text{MD}) + \gamma(\text{tail})$ . The units of temperature are kelvin, g/cm<sup>3</sup> for densities, and mN/m for surface tension.

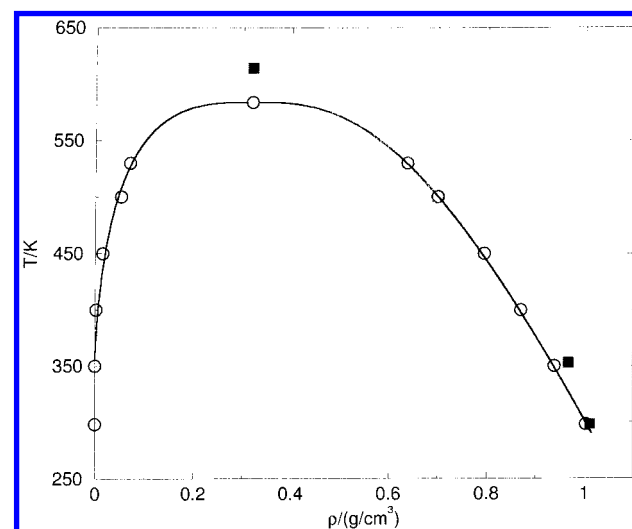


**Figure 6.** Liquid and vapor coexisting densities of MEA. The open circles are CMD results of this work; squares are the experimental values from ref 31. The line is obtained using eq 6 by fitting the CMD results to the rectilinear diameters law. Our critical point is also shown with an open circle. The experimental critical point is taken from ref 2.

to the full potential. In contrast, long-range corrections can be added to the surface tension at the end of the simulation.

We calculated coexisting densities and surface tension as functions of temperature. The densities were obtained using the molecular density profiles. The density profiles, not shown, were calculated using eq 4. The profiles have liquid and vapor phases coexisting through an interface. The simulated bulk phases extend for more than 30 Å, and the interface is stable during the simulation. The liquid and vapor densities are obtained after fitting the profiles to a hyperbolic tangent function by eq 5 at the end of the simulation. By changing the temperature, we obtained the orthobaric curve. The liquid and vapor densities as functions of temperature are given in Table 3, and they are also shown in Figure 6.

Our calculated densities are compared with available experimental results. The simulated liquid density at 298 K is 1.003 g/cm<sup>3</sup> versus the experimental value<sup>30,31</sup> of 1.012 g/cm<sup>3</sup>.

By using the subcritical simulation data, ranging from 350 to 530 K, the critical point is estimated using the eq 6 with constants  $B_0 = 1.18$ ,  $B_1 = 0.13$ , and  $C_2 = 0.37$ . The critical density is 0.32 g/cm<sup>3</sup>, and the critical temperature is 583.9 K. The experimental values are 0.3116 g/cm<sup>3</sup> and 614 K, respectively.<sup>2</sup> The calculated critical temperature is 5% below the experimental data.

The surface tension was obtained using eqs 7–14. The results of  $\gamma$  as a function of temperature are given in Table 3 and also shown in Figure 7. Although the large cutoff was used in the interface simulations, the long-range corrections to the surface

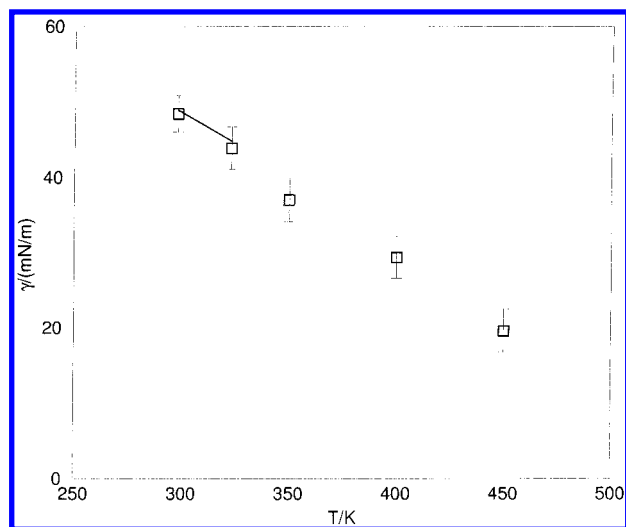


**Figure 7.** Surface tension of MEA. The continuous line is for experimental values from ref 30, and open squares are MD results of this work. The error bars are included.

tension are 15% for temperatures lower than 400 K. The agreement with available experimental data is rather good.

In many applications, MEA is used below 400 K; this force field can be used to obtain transport properties or to simulate MEA in aqueous solutions. More experimental information is needed to improve, at high temperatures, the force field presented in this work.

## VI. Conclusions

Using ab initio calculations in the vapor phase combined with molecular dynamics simulations in condensed phases, we developed a force field for monoethanolamine to be used in molecular simulations. A good starting point to calculate the atomic charges is to match the experimental dipole moment and molecular geometry. The force field is validated over a wide range of temperatures by calculating the surface tension and coexisting densities for liquid–vapor equilibrium.

The force field gives a good description of hydrogen-bonding formation; the hydrogen of the hydroxyl group associates electrostatically with a nitrogen of the amino group and with the oxygen of the hydroxyl group. The hydrogen of the amino group does not favor hydrogen bonding with oxygen or nitrogen atoms from other molecules. The hydroxyl group in MEA has similar hydrogen-bonding behavior to water.

The proposed force field reproduces the available experimental liquid and vapor densities and the surface tension. Our critical temperature and surface tension at 323 K are, respectively, 6% and 4% lower than the experimental values.

**Acknowledgment.** V. d. l. G. thanks IMP for a scholarship; J.A. thanks IMP for computing time and CONACYT for financial support. We thank Dr. Artruro Trejo of IMP for motivating us to work in this interesting subject. We also thank Professor J.J. dePablo and V. Romero-Rochín for carefully reading the manuscript.

## References and Notes

- (1) Kirk-Othmer; *Encyclopedia of Chemical Technology*, 3rd ed.; John Wiley and Sons: New York, 1978, Vol. 1.
- (2) Reid, R.C.; Prausnitz, J. M.; Poling, B. E. *Properties of gases and liquids*; 4th ed.; McGraw-Hill: New York, 1987; p 667.
- (3) Diguillo, M.; Lee, R. J.; Shaeffer, S. T.; Brasher, L. L.; Teja, A. S. Densities and viscosities of the ethanolamines. *J. Chem. Eng. Data* **1992**, 37, 239.

- (4) Diguillo, M.; McGregor, L.; Teja, A. S. Thermal conductivities of ethanolamines. *J. Chem. Eng. Data* **1992**, 37, 242.
- (5) Isaacs, E. E.; Otto, F. D.; Mather, A. E. Solubility of mixtures of H<sub>2</sub>S and CO<sub>2</sub> in monoethanolamine solution at low partial pressures. *J. Chem. Eng. Data* **1980**, 25, 118.
- (6) Blauwhoff, P. M.; Versteeg, G. F.; Swaaij, W. P. V., A study on the reaction between CO<sub>2</sub> and alkanolamines in aqueous solutions. *Chem. Eng. Sci.* **1984**, 39, 207.
- (7) Penn, R. E.; Curl, R. F., Jr. Microwave spectrum of 2-aminoethanol: structural effects of the hydrogen bond. *J. Chem. Phys.* **1971**, 55, 651.
- (8) Berendsen, H. J. C.; Grigera, J. R.; Straatsma, T. P. *J. Phys. Chem.* **1987**, 91, 6269.
- (9) Jorgensen, W. L.; *J. Am. Chem. Soc.* **1981**, 103, 335.
- (10) Button, J. K.; Gubbins, K. E.; Tanaka, H.; Nakanishi, K. Molecular dynamics simulation of the hydrogen bonding in monoethanolamine. *Fluid Phase Equilib.* **1996**, 116, 320.
- (11) Panagiotopoulos, A. Z. Direct determination of phase coexistence properties of fluids by Monte Carlo simulation in a new method. *Mol. Phys.* **1987**, 61, 813.
- (12) Escobedo, F. A.; de Pablo J. J. Expanded grand canonical and Gibbs ensemble Monte Carlo simulation of polymers. *J. Chem. Phys.* **1996**, 105, 2703.
- (13) Kofke, D. A. Direct evaluation of phase coexistence by molecular simulation via integration along the saturation line. *J. Chem. Phys.* **1993**, 98, 4149.
- (14) Lie, G. C.; Grigoras, S.; Dang, L. X.; Yang, D.-J.; Mclean, D. J. *J. Chem. Phys.* **1993**, 99, 3933.
- (15) Alejandre, J.; Tildesley, D. J.; Chapela, G. A. *J. Chem. Phys.* **1995**, 102, 4574. Molecular dynamics simulation of the orthobaric densities and surface tension of water.
- (16) Harris, J. G. *J. Phys. Chem.* **1992**, 96, 5077. Liquid–vapor interfaces of alkane oligomers. Structure and thermodynamics from molecular dynamics simulations of chemically realistic models.
- (17) Trokhymchuk, A.; Alejandre, J. *J. Chem. Phys.* **1999**, 111, 8510. Computer simulations of liquid–vapor interface in Lennard-Jones fluids: Some questions and answers.
- (18) Alejandre, J.; Tildesley, D. J.; Chapela, G. A. *Mol. Phys.* **1995**, 85, 651. Fluid-phase equilibria using molecular dynamics: The surface tension of chlorine and hexane.
- (19) Matsumoto, M.; Takaoka, Y.; Kataoka, Y. *J. Chem. Phys.* **1993**, 98, 1464. Liquid–vapor interface of water–methanol mixture. I. Computer simulation.
- (20) Taylor, R. S.; Garret, B. C. *J. Phys. Chem. B* **1999**, 103, 884. Accommodation of alcohols by the liquid–vapor interface of water: Molecular dynamics study.
- (21) Potter, S. C.; Tildesley, D. J.; Burges, A. N.; Rogers, S. C. *Mol. Phys.* **1997**, 92, 825. A transferable potential model for the liquid–vapor equilibria of fluoromethanes.
- (22) SPARTAN, wavefunction, Inc. Version 3.1.; 18401 Von Karman Ave. Suite 370, Irvine, CA 92715, 1993.
- (23) Foreman, J. B.; Frisch, A. *Exploring chemistry with electronic structure methods*, second ed.; Gaussian, Inc.: Pittsburgh, PA, 1993.
- (24) Frisch, M. J.; Trucks, G. W.; Schlegel, H. B.; Gill, P. M. W.; Johnson, B. G.; Robb, M. A.; Cheeseman, J. R.; Keith, T.; Petersson, G. A.; Montgomery, J. A.; Raghavachari, K.; Al-Laham, M. A.; Zakrzewski, V. G.; Ortiz, J. V.; Foresman, J. B.; Cioslowski, J.; Stefanov, B. B.; Nanayakkara, A.; Challacombe, M.; Peng, C. Y.; Ayala, P. Y.; Chen, W.; Wong, M. W.; Andres, J. L.; Replogle, E. S.; Gomperts, R.; Martin, R. L.; Fox, D. J.; Binkley, J. S.; Defrees, D. J.; Baker, J.; Stewart, J. P.; Head-Gorson, M.; Gonzalez, C.; Pople, J. A. *GAUSSIAN 94*, Revision C.3; Gaussian, Inc.: Pittsburgh, PA, 1995.
- (25) Burgess, A. W.; Shipman, L. L.; Nemenoff, R. A.; Sheraga, H. A. A new approach to empirical intermolecular and conformational potential energy functions. III. Application of EPEN to the conformational analysis of 1,2-disubstituted ethanes. *J. Am. Chem. Soc.* **1976**, 98, 23.
- (26) Ryckaert, J.-P.; Cicotti, G.; Berendsen, J. C. *J. Comput. Phys.* **1977**, 23, 327.
- (27) Vega, L.; de Miguel, E.; Rull, L. F.; Jackson, G.; McLure, I. A. Phase equilibria and critical behavior of square-well fluids of variable width by Gibbs ensemble Monte Carlo simulation. *J. Chem. Phys.* **1992**, 96, 2296.
- (28) Chialvo, A. A.; Cummings, P. T. Engineering a simple polarizable model for the molecular simulation of water applicable over wide ranges of state conditions. *J. Chem. Phys.* **1996**, 105, 8274.
- (29) Soper, A. K.; Phillips, M. G. A new determination of the structure of water at 25 °C. *Chem. Phys.* **1986**, 107, 47.
- (30) Vázquez, G.; Álvarez, E.; Navaza, J. M.; Rendo, R.; Romero, E. Surface tension of binary mixtures of water + monoethanolamine and water + 2-amino-2-methyl-1-propanol and tertiary mixtures of these amines with water from 25 °C to 50 °C. *J. Chem. Eng. Data* **1997**, 42, 57.
- (31) Reitmeir, R. E.; Sivertz, V.; Tartar, H. V. *J. Am. Chem. Soc.*, **1940**, 62, 1943.